Mon. Not. R. Astron. Soc. **000**, 000–000 (0000) Printed 8 November 2010 (MN LATEX style file v2.2)

Biases in the Quasar Mass-Luminosity Plane

Alireza Rafiee and Patrick B. Hall
Department of Physics and Astronomy, York University, 4700 Keele St., Toronto, Ontario, M3J 1P3, Canada

8 November 2010

ABSTRACT

We report that the reported sub-Eddington boundary in the quasar mass-luminosity plane (a departure from the Eddington luminosity limit for the highest quasar black hole masses at a given redshift) is an artifact due to biases in black hole mass measurements. The sub-Eddington boundary was initially found by Steinhardt & Elvis (2010a) using the FWHM-based black hole mass catalogue of Shen et al. (2008). However, the significance of the boundary is reduced when the FWHM-based mass-scaling relationship is recalibrated following Wang et al. (2009) and using the most updated reverberation mapping estimates of black hole masses. Furthermore, this boundary is not seen using mass estimates based on the line dispersion of the same quasars' Mg II emission lines. Thus, the initial report of the sub-Eddington boundary was due to biases in estimating masses using the FWHM of a fit of one or two Gaussians to quasar Mg II emission lines. We provide evidence that using the line dispersion of the Mg II line produces less biased black hole mass estimates.

Key words: black hole physics — galaxies: evolution — galaxies: nuclei — quasars: general — accretion, accretion discs

1 INTRODUCTION

Steinhardt & Elvis (2010a) (hereafter SE10a; see also Steinhardt & Elvis 2010bc) have claimed that there exists a departure from the Eddington luminosity (L_{Edd}) boundary for the highest quasar black hole masses at a given redshift, which they term a sub-Eddington boundary (SEB). SE10a investigated the authenticity of the SEB and argued that the presence of the SEB found in the Shen et al. (2008) data set is neither due to measurement error nor due to small number statistics.

SE10a use the black hole (BH) masses of Shen et al. (2008), who adopted mass scaling relations for Hβ and C IV from Vestergaard & Peterson (2006) and for Mg II from McLure & Dunlop (2004). Both those references have assumed a tight relationship between the radius of the emitting region and the AGN continuum luminosity in the form of $R \propto L^{\alpha}$, where $\alpha \simeq 0.5$, and another relationship between the line width of the emission line, v_{virial}, and the single-epoch FWHM of the same line in the form $v_{virial} \propto$ FWHM. SE10a assume that the presence of the SEB is unlikely to be affected by the above assumptions.

Peterson et al. (2004) suggested that the best indicator for the line width to use when calculating BH masses is the line dispersion of the rms[1] spectrum obtained during a reverberation mapping study. However, because the FWHM of single epoch spectra may not be linearly proportional to the rms σ_{line}, Wang et al. (2009) claim that the relation $v_{virial} \propto$ FWHM may not hold in general and suggest using a relationship of the form $v^2_{virial} \propto \mathrm{FWHM}^{\gamma}$ instead.

Motivated by Wang et al. (2009), we investigate the reliability and biases of the SEB by re-estimating the mass scaling relation and by using two different methods of estimating line width; namely, using the FWHM and the line dispersion of a single epoch spectrum. We present and discuss the SEB in § 2. We compare the use of FWHM- and line dispersion-based BH masses in § 3. We discuss the effects of using different mass scaling relationships on the SEB in § 4. We end with our conclusions in § 5.

2 THE SUB-EDDINGTON BOUNDARY

SE10a have plotted the mass-luminosity plane using the black hole masses of Shen et al. (2008) from the SDSS DR5 quasar sample (Schneider et al. 2007). They have used 62185

[1] The mean spectrum can be defined as $\overline{F(\lambda)} = \frac{1}{N}\sum_{i=1}^{N} F_i(\lambda)$ where $F_i(\lambda)$ is the ith spectrum of the N spectra that compose the reverberation data for one object. The rms spectrum can be defined as $S(\lambda) = \left\{\frac{1}{N-1}\sum_{i=1}^{N}[F_i(\lambda) - \overline{F(\lambda)}]^2\right\}^{1/2}$ (Peterson et al. 2004). The rms FWHM or rms line dispersion is that quantity extracted from the rms spectrum.

quasars over the redshift range $0.2 < z < 4.0$ with three BH mass scaling relations using the FWHMs of the Hβ, Mg II, and C IV emission lines.

SE10a divide their Hβ, Mg II, and C IV mass estimates into 13 redshift bins (though their conclusions are only based on Hβ and Mg II). They show that the SEB is a prominent feature in most of the bins, especially the highest redshift ones. The Mg II emission line can be measured from SDSS spectra in eight of these redshift bins.

In Figure 1a, we reproduce the SEB found by SE10a using the Shen et al. (2008) quasar BH masses. The gap between the red-dashed line (the area below an Eddington ratio of one), the solid-blue line (defining the limits of the observed distribution), and the saturation limit (upper horizontal dash-dotted line) is called the sub-Eddington boundary.

In Figure 2 panels (a) to (h), we use the same quasar sample as Figure 1a but plot the mass-luminosity plane for 8 redshift bins between $0.76 < z < 1.98$. Based on a similar diagram (their Figure 8, panels 4 to 11), SE10a concluded that the most luminous low-mass quasars in any given redshift bin *are* at the Eddington limit but that the most luminous high-mass quasars are *not* at the Eddington limit.

However, the SEB cannot be seen using the Rafiee & Hall (2010) BH mass catalogue which is based on the line dispersion of Mg II instead of its FWHM. We have plotted the mass-luminosity plane for the same objects but using the Rafiee & Hall (2010) BH mass estimate in Figure 1b and in Figure 3 panels (a) to (h). These plots show no evidence for the existence of the SEB.

We have shown that two BH mass samples from essentially the same SDSS data set yield different results. The fact that different mass-scaling relations were used for these samples suggests that the SEB is sensitive to either the mass calibration or the line width indicator used. We now proceed to investigate these issues.

3 DISCUSSION

Shen et al. (2008) fit Mg II as a sum of two Gaussians, one constrained to have FWHM$<$1200 km s^{-1}, and use the FWHM of the broader Gaussian as the Mg II FWHM. It is convenient to assume that quasar emission lines can be modeled as sums of two Gaussians; however, the validity of this Gaussianity assumption has not yet been fully investigated. There are only a few studies on the non-Gaussianity of quasar broad emission lines in the context of BH mass estimation. Peterson et al. (2004) have suggested using the line dispersion and not the FWHM of the emission profile for mass measurments for several reasons including the Gaussianity assumption. Collin et al. (2006) have used both the FWHM and rms line dispersion of reverberation-mapped AGN to investigate the Gaussianity of the lines. They reported two classes of objects according to the value of FWHM/σ_{line}: Pop. I with values below the Gaussian ratio of $2\sqrt{2\ln 2} \simeq 2.35$ and Pop. II with values above it. Peterson (2007) have also reported that for Hβ this ratio spans $0.71 < \mathrm{FWHM}/\sigma_{line} < 3.45$ with an average ratio of 2.0, indicating that the emission lines may not be well fit by single or double Gaussians.

We have investigated the significance of the Gaussianity assumption for BH mass estimates using the FWHM reported by Shen et al. (2008) and the line dispersion σ_{line} of the same objects from Rafiee & Hall (2010). In Figure 4, we have plotted the histogram of the Mg II FWHM/σ_{line} distribution for our sample of 27728 quasars in the redshift range $0.7 < z < 2.0$. We report a range of $1 < \mathrm{FWHM}/\sigma_{line} < 5$ with a mean value of 2.7 and a mode of 2.55 (the blue dash-dotted line in Figure 4).

In Figure 5, we show contour plots of the distribution of these two Mg II line width indicators as a function of their ratio. There is a strong correlation of FWHM with the ratio FWHM/σ_{line}, but no significant correlation for σ_{line}. As one looks at quasars with increasing Mg II emission line FWHMs, the shape of those lines changes systematically. The change in the typical shape of the Mg II emission-line with FWHM calls into question the use of a BH mass relation calibrated to the FWHM.

In Figure 6, we show contour plots of quasar BH masses versus FWHM/σ_{line} for three scenarios. Panel (a) shows the Shen et al. (2008) results which assume a Gaussian profile for Mg II, and panel (b) the Rafiee & Hall (2010) results which directly use the line dispersion. Figure 6a shows that the dependence of FWHM on the FWHM/σ_{line} ratio means that a broader range of BH masses are found using FWHM-based estimation as compared to σ_{line}-based estimation (Figure 6b). Figure 6c shows that the recalibration of FWHM-based masses discussed in the next section helps to reduce the discrepancy between the range of BH masses estimated using FWHMs and that estimated using σ_{line} values.

4 RECALIBRATING THE BLACK HOLE MASS SCALING RELATION

Wang et al. (2009) have studied the mass scaling relations for the Hβ and Mg II emission lines in 29 out of 35 low redshift AGNs for which Peterson et al. (2004) have reported mass estimates made through reverberation mapping (RM) (see Table 1). In determining new mass-scaling relations, they have assumed a more flexible relation between the virial line width and the FWHM in the form of $v^2_{virial} \propto \mathrm{FWHM}^{\gamma}$ where γ is not fixed at 2, as in conventional virial relations, but rather is a free parameter.

We investigated possible mass scaling relations by using different regression fitting algorithms to estimate the parameters of the best fitting line. However, we base our conclusions on the MLINMIX_ERR method (Kelly et al. 2007), also used by Wang et al. (2009) which we report in Table 1. The MLINMIX_ERR method is preferred over other methods because it is the only fitting method which takes intrinsic scatter and uncertainties in both parameters into account. It should be the default fitting method in such cases, though its results may not differ significantly from other methods for two-parameter fits. We also use another Metropolis-Hastings Markov chain Monte Carlo simulation (MCMC; Haario et al. 2006) which gives very similar results to LINMIX_ERR and MLINMIX_ERR; they both use the Bayesian approach to the regression problem but use different sampling algorithms. The MCMC and MLINMIX_ERR (and LINMIX_ERR) simulations yield confidence levels as well as potential outliers and the distribution of the accept-

able parameters and their associated errors within the parameter space.

Other methods used in previous studies are less sophisticated. For example, the BCES method (Akritas & Bershady 1996, e.g., used by McLure & Dunlop 2004, Kaspi et al. 2005, Vestergaard et al. 2006) considers bivariate correlated errors and a possible intrinsic scatter but it does not report that scatter. A quantified value of the intrinsic scatter is available from the FITexy-T02 method (Tremaine et al. 2002, e.g., used by Kaspi et al. 2005, Vestergaard et al. 2006). However, FITexy-T02 does not account for the bivariate correlated errors in the fitting process. Nonetheless, for convenience, we report the results from all these methods in Table 2.

Wang et al. (2009) have adopted the reverberation BH masses of 24 objects in the Peterson et al. (2004) sample. Wang et al. (2009) also included the RM BH masses of 5 objects from more recent reverberation campaigns: NGC 4593 from Denney et al. (2006), NGC 4151 from Metzroth et al. (2006), PG 2130+099 from Grier et al. (2008), and NGC 4051 from Denney et al. (2009). We take the σ_{line}(Hβ,rms) values of all 29 RM objects from Peterson et al. (2004).

For their full 29-quasar RM sample, Wang et al. (2009) found a different power-law relation between FWHM(Mg II) and σ_{line}(Hβ,rms):

$$\log\left[\frac{\sigma_{line}(\mathrm{H}\beta,\mathrm{rms})}{1000\ \mathrm{km\ s^{-1}}}\right] = (0.85\pm0.21)\log\left[\frac{\mathrm{FWHM(Mg\,II)}}{1000\ \mathrm{km\ s^{-1}}}\right] -(0.21\pm0.12). \quad (1)$$

Based on this result, Wang et al. (2009) concluded that the line-emitting locations of Mg II are different from those of Hβ in the broad line region (BLR). That conclusion may be premature, as the difference from unity slope is $< 1\sigma$ statistical significance and the FWHM(Mg II) values are measured from single epoch spectra and not from the same rms spectra as the σ_{line}(Hβ) values. Nonetheless, they suggest fitting a three parameter relation between $\mathcal{M}_{\rm BH}$, FWHM and λL_{3000}:

$$\log\left[\frac{\mathcal{M}_{\rm BH}(RM)}{10^6\mathcal{M}_\odot}\right] = \alpha+\beta\times\log\left[\frac{\lambda L_\lambda}{10^{44}\ \mathrm{erg\ s^{-1}}}\right] +\gamma\times\log\left[\frac{\mathrm{FWHM(Mg\,II)}}{1000\ \mathrm{km\ s^{-1}}}\right] \quad (2)$$

where $\gamma = 1.7\pm0.42$ provides consistency between Mg II and Hβ.

Motivated by Wang et al. (2009), we have revisited the mass scaling relation used by Shen et al. (2008), which was derived by McLure & Dunlop (2004) based on 20 RM objects studied in McLure & Jarvis (2002). McLure & Dunlop (2004) reported a one-to-one relation between FWHM-based $\mathcal{M}_{\rm BH}$ (Hβ) and $\mathcal{M}_{\rm BH}$ (Mg II), $\log\mathcal{M}_{\rm BH}(\mathrm{H}\beta) = 1.00(\pm0.08)\log\mathcal{M}_{\rm BH}(\mathrm{Mg\,II}) + 0.06(\pm0.46)$ and concluded that Hβ can be replaced by Mg II for purposes of mass estimation.

As a next step, we have updated the BH mass list used by Wang et al. (2009) with the most recent reverberation mapping estimates of NGC 5548 (Bentz et al. 2009) and NGC 3227 (Denney et al. 2010).

Using those updated BH masses, we have recalibrated the Wang et al. (2009) mass relation. Comparing results before and after updating our sample shows no statistically significant change in the fitting results except for those of FITexy.

The three-parameter fitting results change a little after updating the BH mass sample, with some improvement in the value of the correlation coefficient. This improvement means that the regression line fits the updated sample better than that of Wang et al. (2009) or McLure & Jarvis.

Here, we report the three parameter mass scaling relations using the most updated RM masses and the MLINMIX_ERR regression package.

$$\log\left[\frac{\mathcal{M}_{\rm BH}(RM)}{10^6\mathcal{M}_\odot}\right] = (1.25\pm0.22)+(0.51\pm0.08) \times\log\left[\frac{\lambda L_\lambda}{10^{44}\ \mathrm{erg\ s^{-1}}}\right] +(1.27\pm0.40)\times\log\left(\frac{\mathrm{FWHM(Mg\,II)}}{1000\ \mathrm{km\ s^{-1}}}\right) \pm\sigma_{\log[\mathcal{M}_{\rm BH}/10^6\mathcal{M}_\odot]}(\mathrm{statistical}) \pm(0.15\pm0.5)\ \mathrm{dex(intrinsic\ scatter)}. \quad (3)$$

where $\sigma_{\log[\mathcal{M}_{\rm BH}/10^6\mathcal{M}_\odot]}$(statistical) is the statistical error of the black hole mass from:

$$\sigma_{\log[\mathcal{M}_{\rm BH}/10^6\mathcal{M}_\odot]} = [0.048+0.0012\ (\ln(\ell))^2+0.048\,\frac{{\sigma_\ell}^2}{\ell^2} +0.030\ (\ln(\omega))^2+0.32\,\frac{{\sigma_\omega}^2}{\omega^2}]^{0.5} \quad (4)$$

where $\ell = [\lambda L_{3000}/10^{44}]$ is in units of erg s^{-1}, $\omega = [\mathrm{FWHM}/1000]$ is in units of km s^{-1}, and σ_ω and σ_ℓ are estimated errors from our fitting process. Like Wang et al. (2009), we find that the relationship of $\mathcal{M}_{\rm BH}$ to Mg II FWHM follows a power law with a smaller value than 2 but that the deviation is not statistically significant ($< 2\sigma$).

4.1 Recalibrated Mass-Luminosity Plane

With most of the new mass scaling relations, the sub-Eddington boundary in the mass-luminosity plane is not present.

The Rafiee & Hall (2010) mass-luminosity plane of 8 redshift bins (Figures 3) does not show any SEB for the high redshift bins as was found by SE10a.

The mass-luminosity plane using the Shen et al. (2008) measurements with a re-scaled mass-relation assuming $v^2_{virial} \propto \mathrm{FWHM}^\gamma$ with $\gamma < 2$ shows no sign of a SEB either (see Figure 7). However, the SEB may be a prominent feature if $\gamma \geqslant 2$; as a change from $\gamma = 2$ to $\gamma < 2$ has eliminated the SEB, a change from $\gamma = 2$ to $\gamma > 2$ should strengthen it.

SE10a suggested that any change in mass-scaling relations due to reverberation mass updates or mass scaling recalibration should only shift the locus of quasars in the mass-luminosity plane, moving the quasar locus relative to an Eddington ratio of one. In support of the existence of the SEB, SE10a thus suggested that if the BH mass estimates are incorrect then the quasar locus in the mass-luminosity plane would only be shifted, rather than tilted to fill the SEB gap.

However, our result shows no such monotonic shift in the new mass estimates but rather different shifts in the high and low mass tails of the distribution. Compared to masses

recalibrated with the latest mass-scaling relation, the published Shen et al. (2008) masses overestimate the highest BH masses and underestimate the lowest BH masses. The overall distribution of the log difference of mass is nearly symmetric around zero, as shown in Figure 8a. However, the new mass estimates versus the Shen et al. (2008) masses depicted in Figure 8b show a rotation in the mass distribution around $\log \mathcal{M}_{\rm BH} \sim 9$ instead of a systematic shift in the new mass estimates. This rotation around $\log \mathcal{M}_{\rm BH} \sim 9$ (Figure 8b) may explain the presence of the SEB in the original Shen et al. (2008) data, especially at the highest masses.

5 CONCLUSION

SE10a have argued that the presence of a sub-Eddington boundary (SEB) in the mass-luminosity plane constructed from the Shen et al. (2008) FWHM-based BH mass data set is not due to measurement error and is statistically significant. They have shown that the apparent SEB is not an artifact due to small number statistics.

We have investigated the existence of a SEB using our own data set (Rafiee & Hall 2010) which uses the line dispersion of Mg II to estimate BH masses. Furthermore, motivated by Wang et al. (2009), we have considered the effects of recalibrating the mass scaling relationship using the general three-parameter relation proposed in Equation 2 and taking into account the latest mass updates from reverberation campaigns.

We have found no sign of the SEB in the Rafiee & Hall (2010) data set, before or after recalibration, nor in the recalibrated Shen et al. (2008) data set. We conclude that the presence of the SEB in the original data of Shen et al. (2008) arises from the mass-scaling relation used, and is likely *not* a real boundary.

SE10a ruled out variations in mass-scaling relations as the reason for the SEB by postulating that such variations should result in a systematic shift in the locus of quasars in the mass-luminosity plane. Our studies do not support this suggestion; instead, there is a mass-dependent shift in the mass estimates after recalibration of a mass-scaling relation. For the recalibrations considered here, we see higher mass estimates in the low mass tail and lower mass estimates in the high mass tail of the mass distribution.

REFERENCES

Adelman-McCarthy, J. K., et al. 2007, ApJS, 172, 634
Akritas, M. G., & Bershady, M. A. 1996, ApJ, 470, 706
Bentz, M. C., et al. 2009, ApJ, , 705, 199
Collin, S., Kawaguchi, T., Peterson, B. M., & Vestergaard, M. 2006, A&A, 456, 75
Denney, K. D., et. al. 2006, ApJ, , 653, 152
Denney, K. D., et. al. 2009, ApJ, , 702, 1353
Denney, K. D., et. al. 2010, ApJ, , 721, 715
Grier, C. J., et. al. 2008, ApJ, , 688, 837
Haario, H., Laine, M., Mira, A., & Saksman, E., *Dram: Efficient Adaptive MCMC*, Statistics and Computing, Springer Netherlands 16, no. 4, 339354
Kelly, B. C. 2007, ApJ, , 664, 1489
McLure, R. J., & Jarvis, M. J. 2002, MNRAS, 337, 109
McLure, R. J., & Dunlop, J. S. 2004, MNRAS, 352, 1390
Metzroth, K. G., et. al. 2006, ApJ, , 647, 901
Onken, C. A., & Kollmeier, J. A. 2008, ApJL, 689, L13
Peterson, B. M., et al. 2004, ApJ, , 613, 682
Peterson, B. M. 2007, in The Central Engine of Active Galactic Nuclei, ed. Luis C. Ho & Jian-Min Wang, ASP Conference Series, Vol. 373, 3
Rafiee, A., & Hall, P. B. 2010, ApJS, submitted
Schneider, D. P., et al. 2007, AJ, 134, 102
Shen, Y., Greene, J. E., Strauss, M. A., Richards, G. T., & Schneider, D. P. 2008, ApJ, 680, 169
Steinhardt, C. L., & Elvis, M. 2010, MNRAS, 402, 2637 (SE10a)
Steinhardt, C. L., & Elvis, M. 2010, MNRAS, submitted (arXiv:0911.3155)
Steinhardt, C. L., & Elvis, M. 2010, MNRAS, 406, L1
Sulentic, J. W., Zwitter, T., Marziani, P., & Dultzin-Hacyan, D. 2000, ApJL, , 536, L5
Tremaine, S., et al. 2002, ApJ, 574, 740
Vestergaard, M., & Peterson, B. M. 2006, ApJ, 641, 689
Wang, J.-G., et al. 2009, ApJ, , 707, 1334

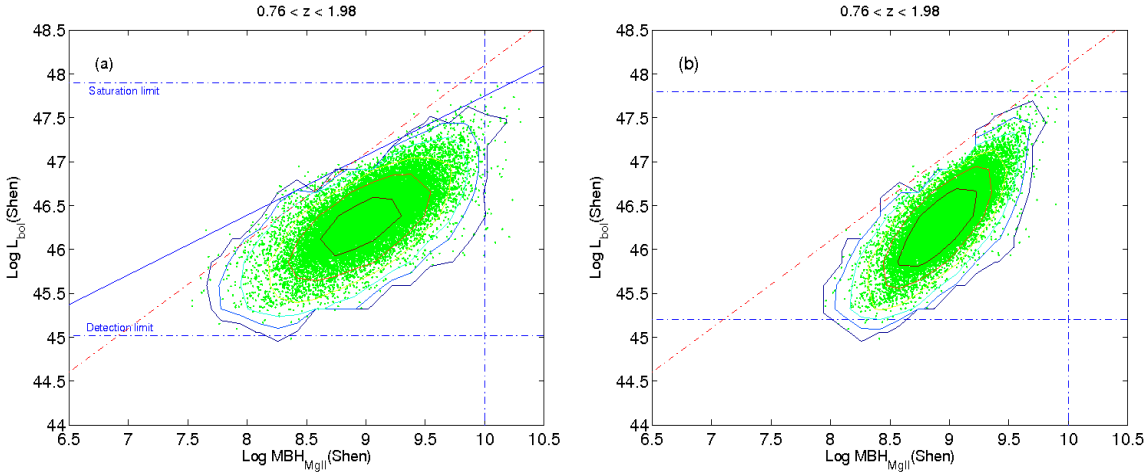

Figure 1. The quasar Mg II mass-luminosity plane, (a) using the original BH masses of Shen et al. (2008), and (b) using the BH masses of Shen et al. (2008) from new mass-scaling relationship of Equation 3. The lower horizontal dot-dashed line is the approximate lower luminosity limit for a low-redshift object at the faint magnitude limit of the SDSS. The upper horizontal dot-dashed line is the upper luminosity limit for a high-redshift object at the bright saturation limit of the SDSS. Objects cannot be detected below the detection limit or above the saturation limit. The vertical dot-dashed line represents an upper mass limit of $\log\mathcal{M}_{\rm BH} = 10$. SE10a have claimed there exists a sub-Eddington boundary: the region between the solid blue line (the edge of the observed distribution) and the red dot-dashed line (an Eddington ratio of one) in panel (a) for objects with $\log\mathcal{M}_{\rm BH} > 9$ at $z \simeq 2$ (solid blue line).

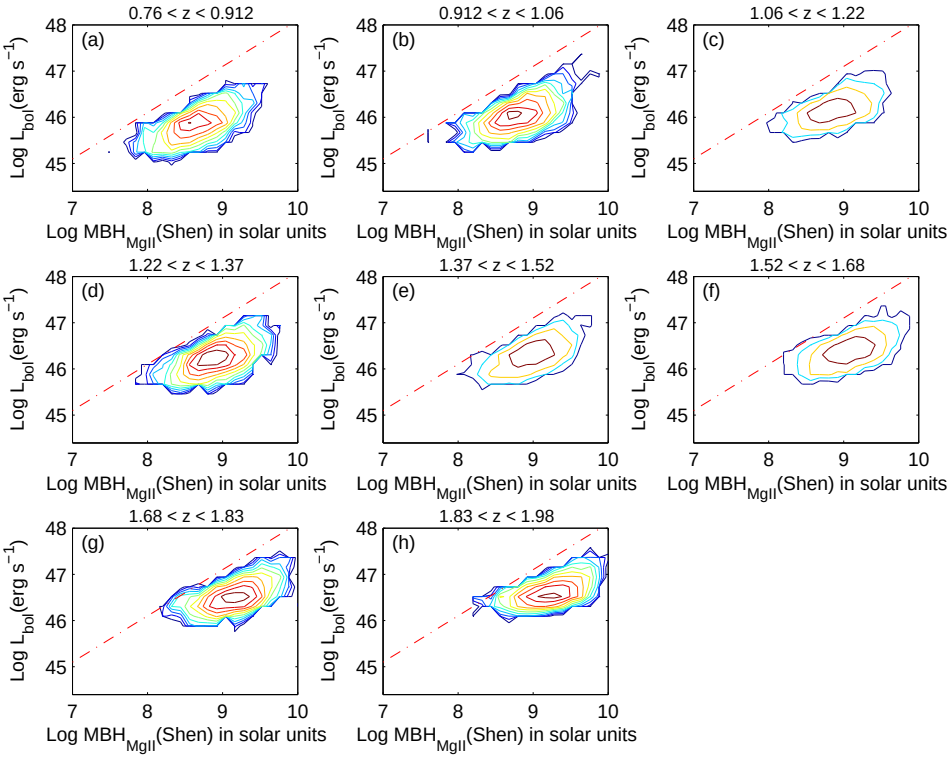

Figure 2. The quasar Mg II mass-luminosity plane for 8 redshift bins using the original BH masses from Shen et al. (2008). A sub-Eddington boundary for objects with the highest $\mathcal{M}_{\rm BH}$ in a given redshift bin can be seen as claimed by SE10a.

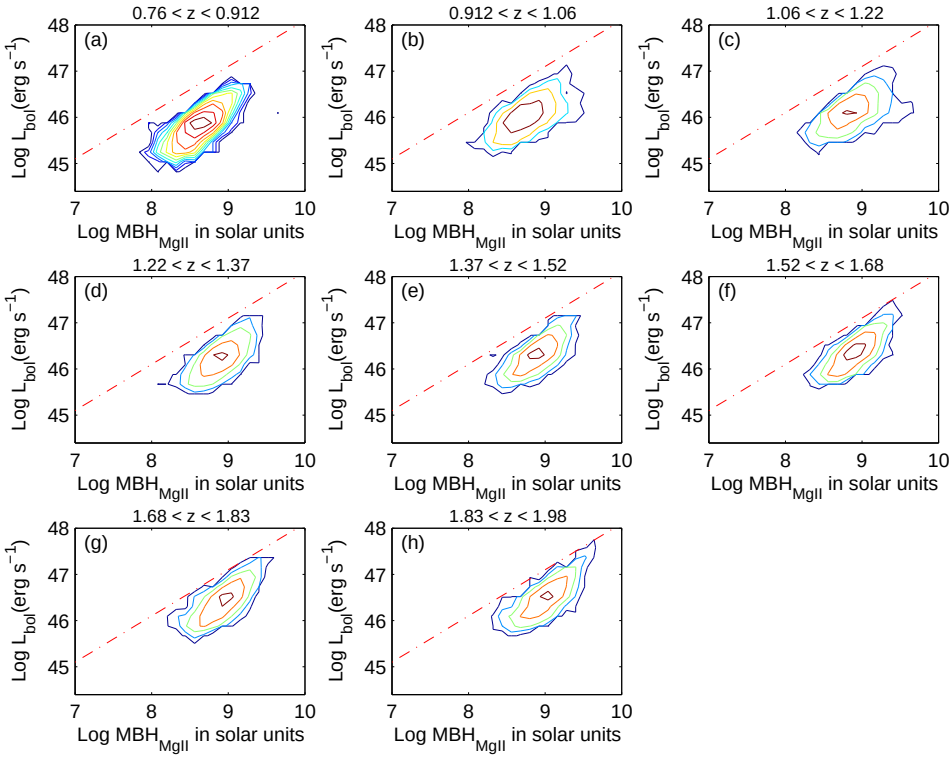

Figure 3. The quasar Mg II mass-luminosity plane for 8 redshift bins when we use the σ_{line}-based BH masses of the Rafiee and Hall (2010) catalogue. The sub-Eddington boundary is not present, particularly in higher redshift bins.

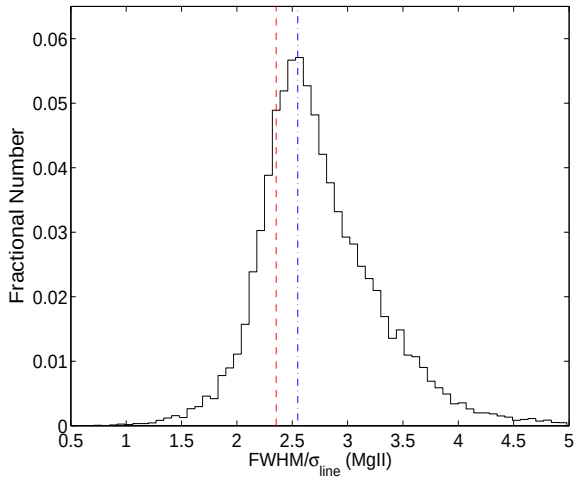

Figure 4. Histogram of $FWHM/\sigma_{line}$ ratios for the Mg II emission line. The FWHM is taken from Shen et al. (2008) and σ_{line} is taken from Rafiee & Hall (2010). The red dashed line represents the value of $2\sqrt{2\ln 2}$ corresponding to a perfect Gaussian profile. The blue dash-dotted line represents the peak at 2.55.

Table 1. Three-parameter fitting results using MLINMIX_ERR (reporting median posterior distribution). $\log(\mathcal{M}_{\rm BH}/10^6\mathcal{M}_\odot) = \alpha + \beta \times \log(\lambda L_\lambda/10^{44}{\rm ergs}^{-1}) + \gamma \times \log(FWHM/1000{\rm kms}^{-1})$.

Data resource	Number of objects	line width	α	β	γ	**Intrinsic Scatter**
Wang et al. 2009	29	FWHM	1.26 ± 0.23	0.46 ± 0.08	1.28 ± 0.42	0.16 ± 0.06
This study (with latest updates on RM mass)	29	FWHM	1.25 ± 0.22	0.51 ± 0.08	1.27 ± 0.40	0.15 ± 0.06

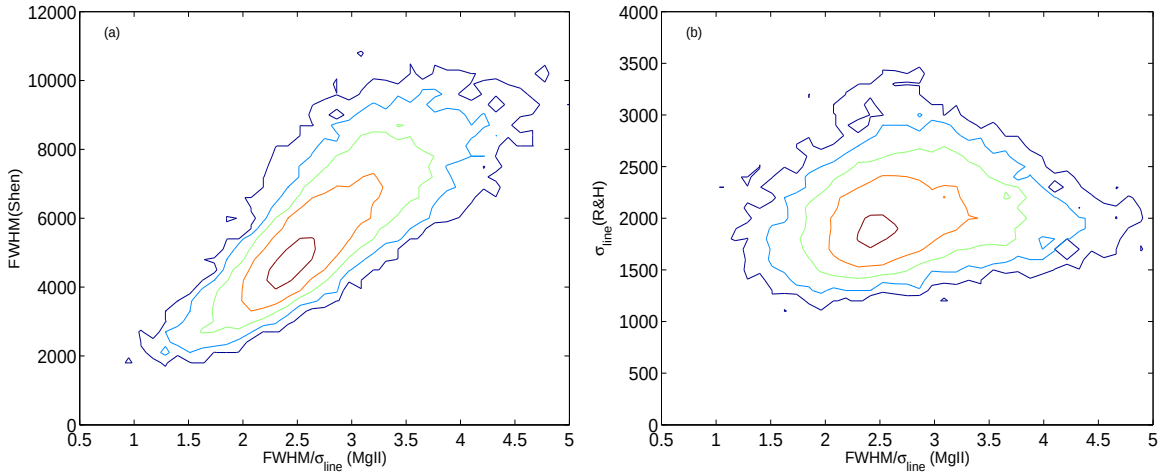

Figure 5. Contour plots of the distributions of two Mg II line width indicators versus their ratio FWHM/σ_{line}. a) Using FWHM from Shen et al. (2008) as the line width indicator. b) Using σ_{line} from Rafiee & Hall (2010) as the line width indicator.

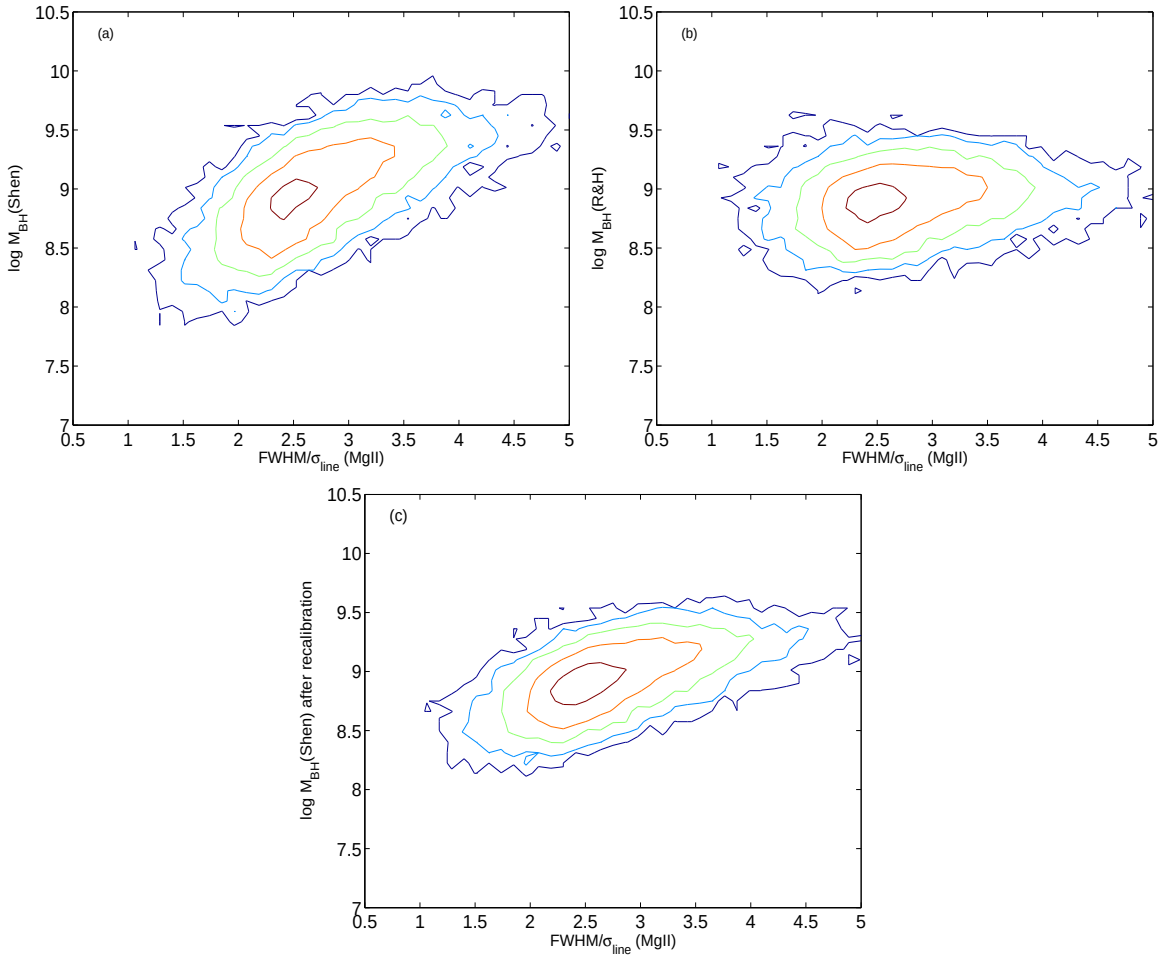

Figure 6. Contour plot of the distribution of log Mg II black hole mass versus FWHM/σ_{line} ratio. a) Using Shen et al. (2008) Mg II BH mass estimates (before recalibration). b) Using Rafiee & Hall (2010) Mg II mass estimates. c) Using the FWHM from Shen et al. (2008) to estimate the BH masses via equation 3. In all plots, the FWHM/σ_{line} ratio uses FWHM from Shen et al. (2008) and σ_{line} from Rafiee & Hall (2010).

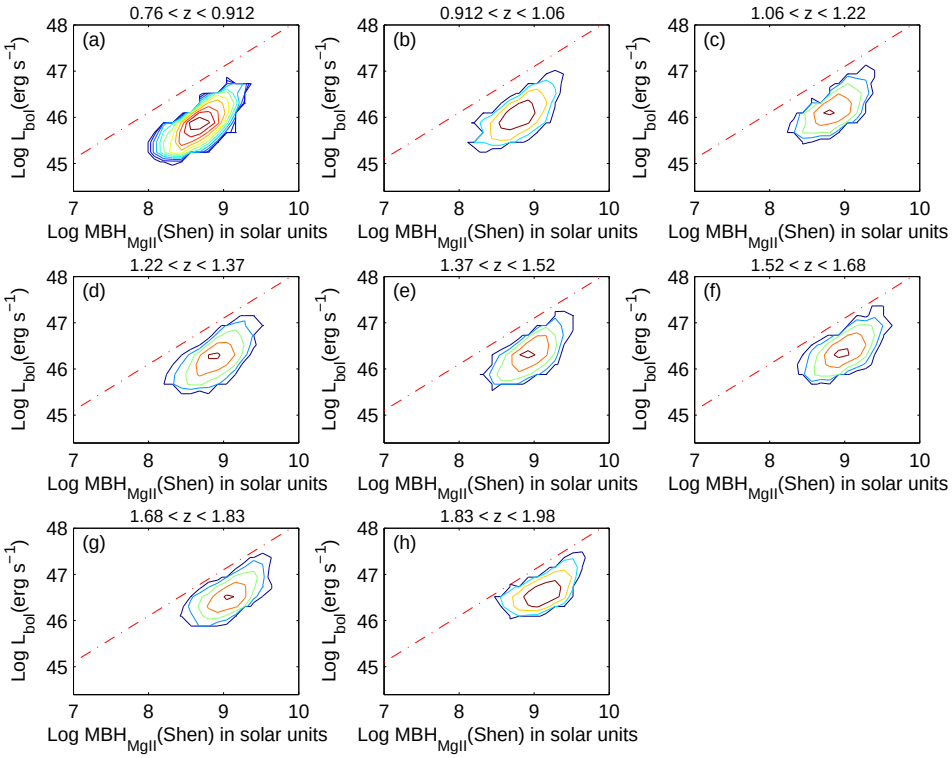

Figure 7. The quasar Mg II mass-luminosity plane for 8 redshift bins when we apply a new mass-scaling relation to the original FWHM and luminosity of Shen et al. (2008). The sub-Eddington boundary has disappeared at high redshift.

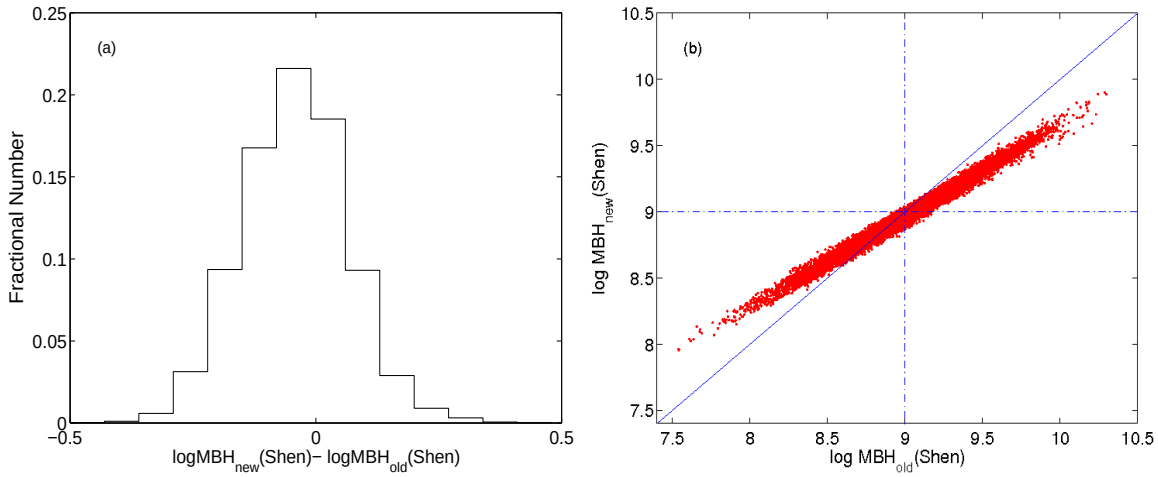

Figure 8. a) The log difference between the Shen et al. (2008) BH masses using the old and new calibrations. There is no systematic shift in the mass distribution. b) Scatter plot of the same BH masses. The mass distribution has rotated around the value $\log \mathcal{M}_{\rm BH} \sim 9$ under the new calibration, causing the SEB to disappear.

Table 2. Re-scaling results using most updated black hole masses. $\log(\mathcal{M}_{\rm BH}/10^6\mathcal{M}_\odot) - 0.5\log(\lambda L_\lambda/10^{44}{\rm ergs}^{-1}) = \alpha + \gamma \times \log(FWHM/1000{\rm kms}^{-1})$.

Fitting Method	Intercept(α)	Slope(γ)	**Intrinsic Scatter**
OLS(Y|X)	1.244 ± 0.25	1.27 ± 0.47	
OLS(X|Y)	-0.136 ± 0.38	3.92 ± 0.66	
OLS Bisector	0.85 ± 0.24	2.03 ± 0.42	
OLS Bisector bootstrap	0.833 ± 0.26	2.05 ± 0.44	
OLS Bisector Jacknife	0.849 ± 0.29	2.03 ± 0.50	
FITexy	0.728 ± 0.09	1.99 ± 0.17	0
FITexy-T02	0.85 ± 0.23	1.95 ± 0.43	0.29
BCES(Y|X)	1.21 ± 0.27	1.34 ± 0.51	
BCES(Y|X) bootstrap	1.16 ± 0.33	1.41 ± 0.60	
BCES(X|Y)	0.0343 ± 0.34	3.95 ± 0.58	
BCES(X|Y) bootstrap	0.203 ± 202.00	3.15 ± 475.00	
BCES Bisector	0.846 ± 0.25	2.03 ± 0.44	
BCES Bisector bootstrap	0.822 ± 0.28	2.07 ± 0.49	
BCES Orthogonal	0.259 ± 0.31	3.16 ± 0.51	
BCES Orthogonal bootstrap	0.346 ± 100.00	2.93 ± 235.00	
MCMC (median posterior distribution)	1.24 ± 0.20	1.28 ± 0.36	0.37 ± 0.05
MCMC (mean posterior distribution)	1.24 ± 0.20	1.27 ± 0.36	0.37 ± 0.05
LINMIX_ERR (median posterior distribution)	1.25 ± 0.22	1.21 ± 0.40	0.11 ± 0.05